Deformable Skin Design to Enhance Response of a Biomimetic Tactile Sensor

Nicholas Wettels *Student Member, IEEE,* Lorenzo M. Smith, Veronica J. Santos, *Member, IEEE*, and Gerald E. Loeb, *Member, IEEE*

***Abstract*— Grasping of objects by robotic hands in unstructured environments demands a sensor surface that is durable, compliant, and responsive to various force and slip conditions. A compliant and robust skin can be as critical to grasping objects as the sensor it protects. In an effort to combine compliant mechanics and robust sensing, a biomimetic tactile sensor is being developed. Deformations of its skin can be detected by displacing a conductive fluid from the vicinity of electrodes on a rigid core. In this study, we used simplified finite element models to understand the effects of various textures for the inner surface of the skin and then produced the more promising textures by molding the elastomeric skin material against negatives made by stereolithography. The impedance vs. force relationships obtained with these molded skins had the predicted and desired wide dynamic range. By selecting the appropriate materials for the skin and fluid, previously described problems with hysteresis and diffusion losses have been greatly reduced.**

I. INTRODUCTION

ONE promising strategy for tactile sensing is based on measuring the deformation of a flexible skin (cosmesis) and an underlying conductive fluid layer by its effect on the impedance of electrodes on the surface of a rigid core structure (Figure 1). Obtaining a useful range of spatial and temporal responses requires that these electrodes function as continuous sensors as opposed to mere switches [1-2]. When a smooth skin surface contacts and occludes a given electrode, a seal is formed isolating it from the fluid and causing impedance to increase to infinity. Texturing of the internal skin surface allows for fluid pathways to exist even after the skin has been compressed against the electrode. Prior work [1] demonstrated that this texturing of the inner surface of the skin extends the dynamic range of the tactile sensor to a physiologically relevant range (0.1-30N). However, the negative mold used to create the textured surfaces in this prior study was commercially-available sandpaper, which had an inhomogeneous distribution of grit. This resulted in an uncontrolled pattern of texturing and inherent repeatability problems due to small lateral shifts between the skin and electrodes.

In this study, systematic design, modeling and testing of candidate skin textures resulted in improved performance of the biomimetic tactile sensor (shown below). Appropriate selections of materials for the skin and fluid were able to resolve previously noted issues of sensor hysteresis and diffusion of fluid through the skin.

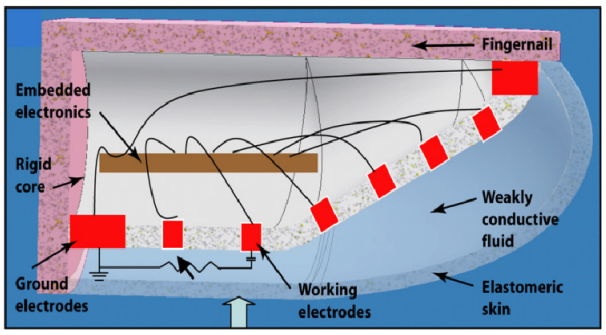

Figure 1: Biomimetic tactile sensing based on impedance changes in a deformable space filled with conductive fluid

II. REVIEW OF LITERATURE

Fluid based tactile sensing in manipulation is not a new concept. Brockett discussed several advantages of robotic manipulanda with fluid-based surfaces [3]. Shimoga and Goldberg provided a comparative analysis of construction materials, including soft ones, for robotic fingertips [4]. Hristu also discussed the advantages of compliant manipulators and simultaneously proposed an optically read gel-filled sensor [5] that had some problems with ambient light. Helsel fabricated a one-dimensional impedance tomographer based on changes in fluid impedance [2], and Russel crafted a uni-axial based sensor using similar technology [6]. Electrorheological based sensors [7,8] use capacitive sensing in conjunction with the compliant gel to form a useful sensor. In general, these approaches have had problems with complexity and robustness.

Other transduction mechanisms such as conductive and piezoelectric polymers, optics and ultrasound have all yielded useful sensitivity but only for limited environments

Manuscript received April 23, 2008. This work was supported by a grant from the National Academies Keck Futures Initiative and by the Alfred E. Mann Institute for Biomedical Engineering at the University of Southern California endowment.

N. Wettels is with the Biomedical Engineering Department, University of Southern California Los Angeles, CA 90089, USA (e-mail: nick.wettels@gmail.com).

V. J. Santos is with Arizona State University Tempe, AZ 85287, USA (email: veronica.santos@)asu.edu)

L. M. Smith is with Oakland University Rochester, MI 48309, USA (email: L8smith@oakland.edu)

G.E. Loeb is with the Biomedical Engineering Department, University of Southern California Los Angeles, CA 90089, USA (phone: 213-821-5311, e-mail: gloeb@usc.edu).

or applications. Skin-like conductive polymeric sensors provide good resolution and sensitivity, but have hysteresis problems [9, 10]. Piezoelectric materials such as PVDF [11] require high impedances that will be difficult to sustain in wet environments. Complex MEMS devices offer tri-axial sensing but place many sensing elements and their delicate connections in an easily damaged location [12]. Polymer-based MEMS may be more robust for use in deformable cosmeses [13] but also require many electrical connections. Surveys of tactile sensing can be found in [14-17]. The recurring theme in this literature is the placement of large numbers of delicate transducers and their connections for power and data in harm's way.

III. METHODS

A. *Finite Element Analysis of Internal Skin Geometry*

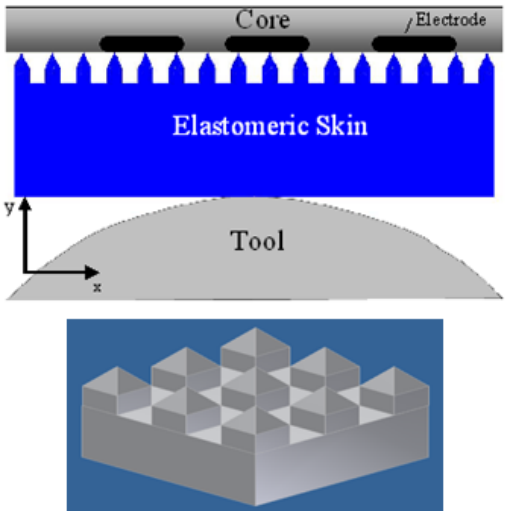

Figure 2: Above) Undeformed two-dimensional geometry for grooved texture, Below) A three dimensional representation of the textured skin

The geometry of the finger-shaped rigid core described in [1] features a curved surface profile with electrodes molded into its surface. In the present analysis (Figure 2), a flat core is assumed for simplicity because the effects of the internal texturing will likely be localized. In the finite element model and the experiment described in the subsequent section, a smooth, rigid tool with a 10mm radius of curvature (ROC) is pressed onto the surface of the outer skin. To model three-dimensional effects accurately, three dimensional analyses must be used. For the purposes of this development step, we used a simplified 2D model (plane stress) to capture the behavior of the proposed 3D asperities, which obviously will be prone to errors due to stresses out of the plane of analysis. We validated the qualitative model results by building and testing flat patches of candidate skin materials with these 3D textures.

A key parameter encountered during the development of the skin texture design was the depth of grooves surrounding and separating the asperities, which would act as channels for the conductive fluid. Finite element analysis (FEA) of modeled skins featuring two design variations were considered as shown in Figure 6. In order to address the texture design effects alone, the skin was modeled and then molded using one skin material type (PMC-744 polyurethane with 45 durometer hardness).

Commercially-available MSC MARC software (Release 2005r3) was used for the FEA simulations. Specifications and modeling settings for the finite element model employed are listed below:

- Element Type: 4-node, Quadrilateral, Plane Stress, Full Integration, (Some elements were degenerated into 3-node elements.)
- Contact: Deformable Workpiece with Rigid 2D Curve for Tool
- Boundary Conditions: Displacement with Applied Rigid Tool Penetration. For all cases, the horizontal (x-direction) displacement for all nodes on the left and right hand side of the deformable skin body were fixed. This constraint was imposed in order to approximate an infinite domain in the x-direction.
- Adaptive Meshing: None.
- Dynamic Effect: None. (Quasi-static)
- Solution Control: Full-Newton Raphson with 180 time steps
- Time Integration: Implicit
- Mesh Refinement: Mesh refinement is based upon a mesh refinement study, where the influences of 3-node element stiffness effects and large element size have been addressed.

Material behavior of the PMC-744 skin is based upon a one-term Mooney's hyperelastic material model, which relates the strain energy density, W, to material coefficients and strain invariants as follows [18]:

$$(1)\quad W = 0.26(I_1 - 3)$$

where: I_1 is the first strain invariant

The material constant, 0.26, is based upon tensile tests in accordance with ASTM standards [19]. A bulk modulus of 22.5 MPa was assumed.

B. *Empirical Testing of Skin Geometries*

In order to create positive features, the uncured two-part elastomer was poured onto negative molds and then centrifuged to remove air bubbles before curing. Molds for two pyramidal geometries (with and without grooves) were produced by stereolithography (Small Parts Inc.).

Strips of the textured skin 13x27mm were tested in a bath with flush-mounted electrodes molded into its flat bottom (Fig. 3). Two 2.5mm diameter platinum electrodes were

embedded in dental acrylic (Hygenic, Perm reline/repair resin). The textured surfaces were systematically pressed against the working electrode using a 10mm ROC probe with a stepper motor while recording forces with a six-axis force plate. The counter-electrode, separated from the working electrode by 15mm, was left uncovered [20]. A .06M solution of propylene glycol/ sodium iodide (resistivity = 6950 Ωcm) was used, as explained in the next section.

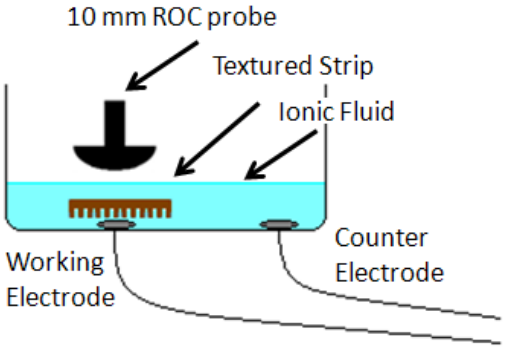

Figure 3: Illustration of texture testing apparatus (not to scale).

The measurement circuit is shown schematically in Figure 4. The system was energized by a 1.6 kHz square-wave and was synchronously sampled by USB-6218 DAQ board. A 1μF capacitor was used to block direct current. The two capacitors represent the electrode-electrolyte interfaces, which present negligible impedance at the test frequency [1, 21]. A 10 kΩ resistor served as a voltage divider, converting the changes in impedance that result from the mechanical deformation of the fluid flow-path into voltages digitized by the DAQ. Fifteen loading/unloading cycles at 8.33mm/s were recorded for each of the skins.

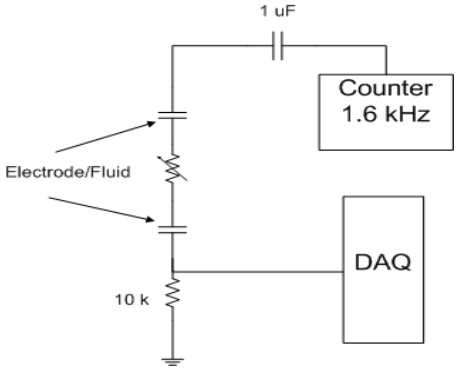

Figure 4: Circuit Diagram of Test Set-up

C. Materials Testing: Diffusion and Hysteresis

In addition to providing a deformable texture for the impedance sensing, the skin must also slide freely over the core and prevent changes in fluid volume as a result of diffusion. Water diffuses fairly readily through silicone, which precludes the use of saline as a transduction medium. Furthermore, during periods of slow loading (< 1 Hz), it was noted that a significant amount of hysteresis developed when the applied force exceeded 3N [1]; this was attributed to static friction between the skin and core. These considerations provided additional constraints on the development of a fluid/skin combination.

The diffusion coefficients were determined for one silicone (Dragonskin (DS) skin and one urethane (PMC-744) skin. Thin, large surface area skins were molded over aluminum rods, cured, peeled from the rods, and filled with test fluid. The skin/fluid sacs were plugged with a small disc of aluminum rod and resealed with their respective elastomers. Weighing occurred at 24 hr intervals over 72 hrs to monitor mass change in a fume hood kept at 75°F (+/- .5F) and 20% humidity (+/- 3.5%).

The goal was to identify a solvent that diffused minimally outward though the elastomer. It had to have sufficient solubility for a salt to provide the desired conductivity but the solution could not be hygroscopic because that might lead to inward diffusion of water in a humid environment. The solution needed to be nontoxic in the event of a breach of the skin. The solvent also had to have sufficient lubricity to reduce the static friction and resulting hysteresis. For the last requirement, we repeated the test configuration described previously [1] in which the skin was PMC-744 textured using 60 grit sandpaper as a negative mold [1]. The skin was tested with 1mL of saline and then with propylene glycol/sodium iodide, the most promising solution based on the other criteria.

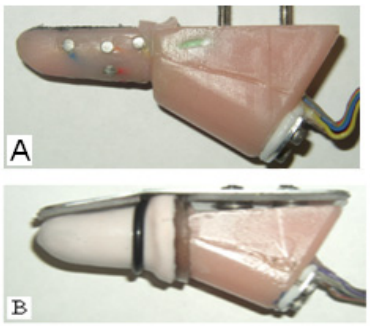

Figure 5: Prototype sensor array: A) Skin removed and platinum electrodes visible; B) Skin and nail installed

IV. RESULTS

A. Finite Element Analysis

The undeformed and deformed geometries of the grooved and non-grooved PMC-744 material are illustrated as predicted by the FEA (Fig. 6). The dimensions of the triangular crown are 0.43mm high and a 23 degree draft angle. The groove depth is 0.43mm with 0.43mm spacing between the structures. As expected during compression, the asperities directly below the center point of the curved tool lean away from each other at the most severe angles. As the

distance from the center of contact increases, the bend angle decreases.

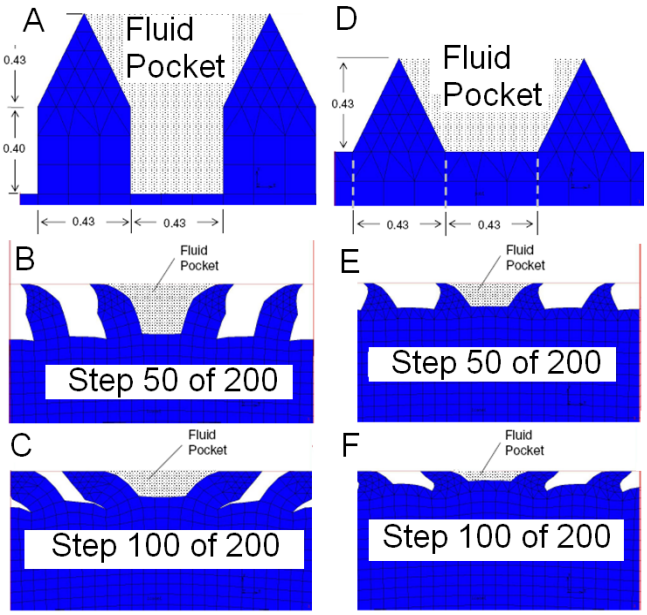

Figure 6: FEA deformation of grooved and non-grooved pyramidal PMC-744 texturing : A)Undeformed grooved model B) Low deformation C) High deformation D) Undeformed non-grooved model E) Low deformation F) High deformation

The inverse of the predicted cross-sectional area of the fluid pocket over the electrode was plotted in Figure 7 as a prediction of the electrical impedance resulting from conduction through that pocket. Results have been normalized with respect to the maximum predicted force and maximum predicted inverse area. During early stages of deformation, the overall slopes of the curves are similar. As deformation progresses, the predicted slopes of the curves depart from one another.

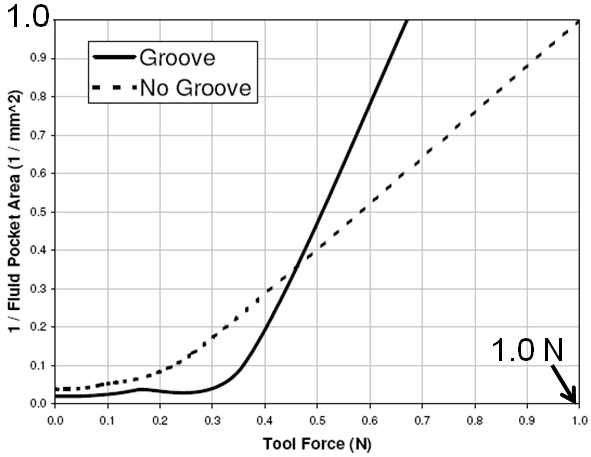

Figure 7: Finite element model results predicting the influence of the tool force on the fluid pocket for PMC-744 textured skin. Results are normalized with respect to the maximum predicted tool force and maximum inverse-area.

B. Empirical Testing of Skin Geometries

In order to confirm the qualitative predictions of the FEA, we photographed the molded asperities as they were compressed under a glass slide (Fig. 8). It is important to note that although the negative molds were designed with sharp features much like the FEA models illustrated in Figure 6, the stereolithographic process used to create the negative molds resulted in substantial rounding, which was faithfully reproduced in the molded elastomer skins.

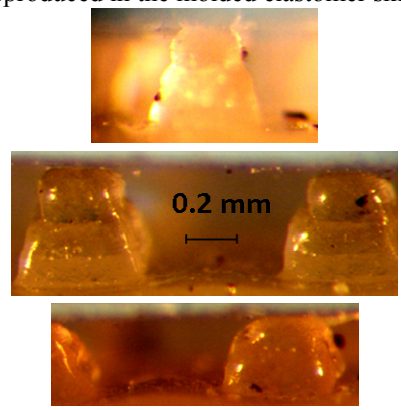

Figure 8: 5X photographs of grooved asperities under varying levels of compression.

In the top picture of Fig. 8 no compression occurs. In the middle figure buckling of the structures occurs. In the bottom picture the tool pushes in the middle of the two asperities, causing compression and one asperity to buckle to the left and the other to the right.

Loading curves are presented for the grooved and ungrooved pyramidal textures in Fig. 11. The grooved structure had a much larger dynamic range, achieving an impedance of 4MΩ at approximately 18N whereas the non-grooved structure achieved the same impedance level at ~10 N. Neither curve shows any sign of saturation at the highest force levels tested.

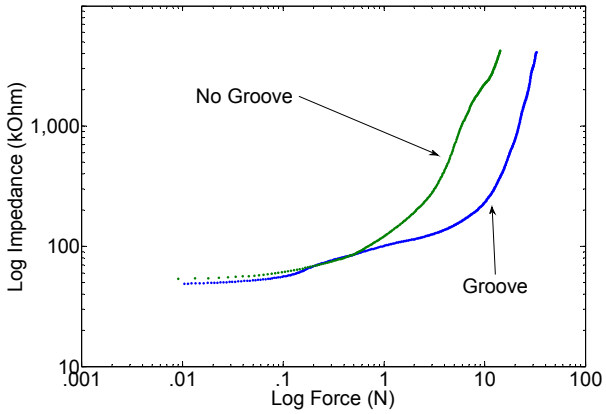

Fig. 9: Loading curves for 45 durometer PMC-744 strips

Six representative curves, three each for the grooved and non-grooved geometries, are shown in Figure 10. The

grooved samples showed less variability between trials than the non-grooved samples, though both samples pose repeatability issues.

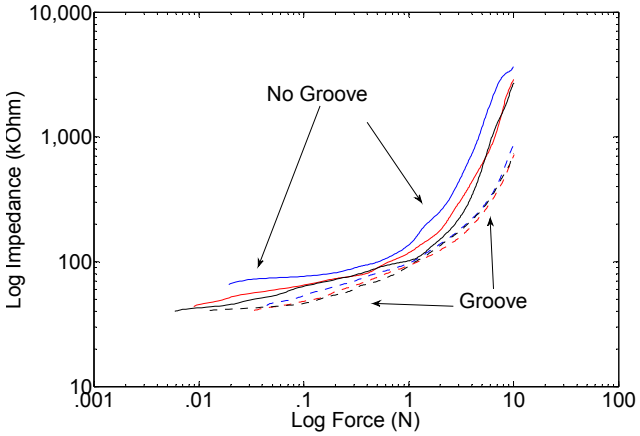

Fig. 10: Repeatability loading curves for Grooved vs. Non-Grooved skin geometries of PMC-744

C. Material Testing: Diffusion and Hysteresis

Hysteresis was calculated from the average of 15 loading/unloading curves of saline and propylene glycol solutions by using log impedances and integrating the difference between the loading and unloading curves divided by the mean of the two curves. This integration was implemented numerically in MATLAB using Simpson's Rule. Hysteresis was 6.20% for the saline solution and 3.35% for the propylene glycol solution.

With respect to diffusion, each of the samples was normalized using the diffusion flux and Fick's First Law [22]. The propylene glycol fluid and silicone skin combination resulted in the lowest diffusion coefficient (Table 1).

Table 1: 72 hour diffusion test results for various fluid/skin combinations

Fluid/Elastomer Skin	Initial Weight (g)	% Normalized Mass Change	Diffusion Coefficient (x 10^{-9} cm^2/s)
PG/ DS	15.605	-.98%	0.386
PG/ PMC-744	14.560	-6.70%	2.18
Water/ DS	15.830	-9.98%	3.88
Water/ PMC-744	12.624	-27.70%	8.51

V. DISCUSSION

A. Finite Element Analysis

A rigorous numerical model of the electromechanical properties of the finger would require calculation of the impedance based upon the geometry of the deformed fluid flow path in a full 3D FEA. Such models are extremely complex to build and would require even more effort to validate. To circumvent such complexities, several recent two-dimensional models have been offered in literature [23-25]. The proposed two-dimensional model represents an amendment to the current body of models available. The experimental results validate the utility of modeling the electromechanical behavior of the texture asperities in this highly simplified way. The models capture the transitions in slope of impedance vs. force and their relative position for the grooved vs. ungrooved designs for the asperities, although they diverge from the measured trends for the higher compression forces. There are many potential sources of error in the FEA models, including uncertainties in the shapes of the asperities as actually molded and the various simplifying assumptions in the construction of the model, particularly regarding Mesh Refinement, Boundary Conditions, Level of Analysis (i.e. two-dimensional or three-dimensional analysis), Element Formulation and limitations of the plane stress model.

B. Empirical Testing of Skin Geometries

The grooved skin made from 45 durometer material (PMC-744) yielded the desired dynamic range for a biomimetic tactile sensor [1]. From Fig. 9, the grooved and ungrooved textures have comparable sensitivity to force, but the grooved structure has a wider dynamic range. This is due to the fact that the grooving provides a deeper channel and a larger flow-path for ions at a given force. Non-grooved pyramids of the same height as the grooved structures may have a similar range and are worth exploring, but the advantage of the grooved structures is that more asperities per area can be placed on the skin than in a regular pyramidal scheme. This is important because higher asperity density will minimize noise. If there are too few asperities per electrode, then the manner in which an incident object contacts the skin or small lateral shifts of the skin position in relation to the electrode can produce artifactual fluctuations (noise) in the measured impedance. It appears from Figure 10 that repeatability due to this type of noise is a problem. The grooved asperities seem to have less variability than the non-grooved structure. Importantly, the uncertainty for this sensor will manifest itself in the perceived force output as opposed to the impedance. At some places, the variability between curves approaches 15%, which may not be acceptable for some applications. Several factors may contribute to this variability: 1) the existing molds were made near the tolerance limits of the stereolithographic technique used to make them (0.38mm feature tolerance), causing theoretically pointed structures to have a radius; 2) The pouring of the liquid elastomers was not done under vacuum conditions, possibly trapping bubbles in the structures, particularly at the tips of the asperities; 3) The number of asperities per electrode is small. Finer asperity patterns will require finer molds as can be produced by numerically-controlled micromachining.

VI. CONCLUSION

Construction of a simple but useful two-dimensional finite element model followed by physical construction and experimental validation resulted in substantial improvements in the performance of force sensors based on measuring the impedance of a conductive fluid trapped beneath a deformable elastomeric skin. Such modeling can be used to screen efficiently a wide range of design alternatives before building physical structures.

Previously noted problems of diffusion and hysteresis have been greatly reduced. Skins made from silicone elastomer and fluids based on propylene glycol appear to solve the diffusion problem. A silicone fingertip with $3cm^2$ surface area, 3mm skin thickness and 1cc of propylene glycol would lose ~10% of its volume in 4 months; this can be easily replaced as required through a resealable injection port. The improvement in lubricity is promising but needs to be assessed during loading by non-normal forces, which are supposed to produce sliding motion of the skin to change the impedance pattern measured by the lateral electrodes as well [1]. Further improvements in both diffusion and lubricity may be possible by creating a gel of the internal solution with a lubricant (e.g. methyl cellulose), but increases in viscosity could reduce the sensitivity to rapid transients of loading and unloading.

ACKNOWLEDGMENTS

The authors would like to thank Mercedes Perez for assistance with chemistry laboratory work, data collection and diffusion analysis, Matt Borzage for numerical analysis, Jeremy Fishel for discussions regarding finite element analysis and Ray Peck for guidance in building the experimental set-up.

REFERENCES

[1] N. Wettels, V. J. Santos, R. S. Johansson, and G. E. Loeb, "Biomimetic tactile sensor array." *Advanced Robotics*, vol. 22, no. 7, June 2008.

[2] M. Helsel, J. N. Zemel, and V. Dominko, An impedance tomographic tactile sensor. *Sensors and Actuators*, **14**:1, pp 93-98, (1988).

[3] R.W. Brockett, Robotic Hands With Rheological Surfaces, Proceedings of the IEEE Conference on Robotics and Automaton, Philadelphia, PA, pp. 942–946 (1985)

[4] K.B. Shimoga and A.A. Goldenberg Soft Robotic Fingertips: Part I: A Comparison of Construction Materials *The International Journal of Robotics Research*; Vol 15; No. 320, 1996

[5] D. Hristu N. Ferrier R.W. Brockett, The performance of a deformable-membrane tactile sensor: basic results on geometrically-defined tasks. *Proc of the IEEE International Conference on Robotics & Automation* San Francisco, CA (2000)

[6] Russell, R.A., Parkinson, S. Sensing Surface Shape by Touch, *Proceedings of IEEE International Conference on Robotics and Automation* Atlanta, GA pp. 423 – 428 (1993)

[7] G. Kenaley, M. Cutkosky Electrorheological Fluid-Based Robotic Fingers with Tactile Sensing *1996 IEEE International Conference on Robotics and Automation* p 132-136, Scottsdale, AZ (1989)

[8] R. M. Voyles, G. Fedder, and P.K. Khosla Design of a Modular Tactile Sensor and Actuator Based on an Electrorheological Gel, *Proc of the IEEE International Conference on Robotics and Automation*, Minneapolis, MN (1996).

[9] M. Shimojo et al. A Tactile Sensor Sheet Using Pressure Conductive Rubber With Electrical-Wires Stitched Method, *IEEE Sensor Journal,* Vol. 4, No. 5, pp. 589 – 596, (2004)

[10] T. Jensen, R. Radwin, J. Webster, A Conductive Polymer Sensor for Measuring External Finger Forces *J. Biomechanics* Vol. 24. No. 9. pp. 851-858, (1991)

[11] Shinoda and S. Ando, Ultrasonic Emission Tactile Sensor for Contact Localization and Characterization, Proc of International Conference on Robotics and Automation, San Diego, CA (1994)

[12] J. Engel, J, Chen, Z. Fan and C. Liu, Polymer Micromachined Multimodal tactile Sensors. Sensors and Actuators A 117 pp. 50–61 (2005)

[13] Y. Yamada and M. Cutkosky "Tactile Sensor with 3-Axis Force and Vibration Sensing Functions and Its Application to Detect Rotational Slip", Proc of International Conference on Robotics and Automation , San Diego, CA (1994)

[14] M. H. Lee and H. R. Nichols, Tactile Sensing for Mechatronics – a state of the art survey. *Mechatronics*, 9, 1-31 (1999).

[15] Howe, R.D., "Tactile Sensing and Control of Robotic Manipulation," in *Journal of Advanced Robotics*, Vol.8,No.3, pp. 245-261 (1994)

[16] C. Melchiorri, Tactile Sensing for Robotic Manipulation, in Ramsete: Lecture Notes in Control and Information Sciences Volume 270 Springer Berlin (2001)

[17] Roderic A. Grupen, Thomas C. Henderson and Ian D. McCammon A Survey of General- Purpose Manipulation *The International Journal of Robotics Research*; 8; 38 *(*1989)

[18] Vossoughi, J., "Determination of Mooney Material Constants for Highly Nonlinear Isotropic Incompressible Materials Under Large Elastic Deformations", Experimental Techniques, pp. 24 – 27, 1995

[19] "Standard Test Methods for Vulcanized Rubber and Thermoplastic Elastomers – Tension", ASTM 412-98a, 2002

[20] H.A Ruddy and G.E. Loeb, "Influence of materials and geometry on fields produced by cochlear electrode arrays." *Med. & Biol. Eng. & Comput.* **33,** pp 793-801 (1995).

[21] D. Merrill, M. Bikson, and J. Jeffreys, Electrical stimulation of excitable tissue: design of efficacious and safe protocols, *J. Neurosci. Methods*, **141**, pp 171-198, (2005).

[22] W.D. Calister, Fundamentals of Materials Science and Engineering, An Integrated Approach (2nd Ed.) John Wiley & Sons, Inc. pp 158-9, (2005)

[23] S. L. Ricker, R. E. Ellis, 2D *Finite Element Models of Tactile Sensors*, IEEE, pp. 941 – 947, 1993

[24] V. Grigas, R.T. Tolocka, P. Ziliukas, Dynamic Interaction of Fingertip Skin and Pin of Tactile Device, *Journal of Sound and Vibration*, 308, pp. 447 – 457, 2007

[25] G. Vasarhelyi, B. Fodor, T. Roska, Tactile Sensing-Processing: Interface-cover Geometry and the Inverse-Elastic Problem, *Sensors and Actuators A*:, 140, pp 8 – 18, 2007